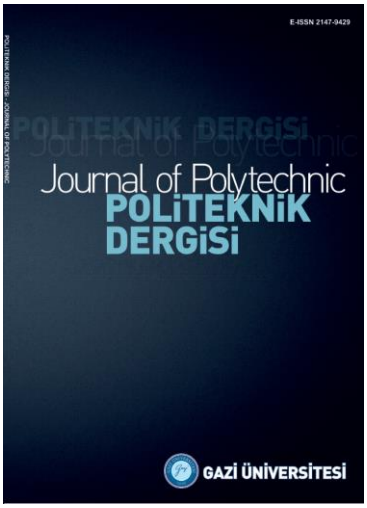

POLİTEKNİK DERGİSİ

JOURNAL of POLYTECHNIC

ISSN: 1302-0900 (PRINT), ISSN: 2147-9429 (ONLINE)
URL: http://dergipark.gov.tr/politeknik

Crystal size and stress account in reciprocal space map

Ters örgü uzayında kristal boyutu ve stres hesabı

Yazar(lar) (Author(s)): *İlknur KARS DURUKAN[1*], Mustafa Kemal ÖZTÜRK[2], Süleyman ÖZÇELİK[3], Ekmel ÖZBAY[4]*

ORCID[1]: 0000-0001-5697-0530

ORCID[2]: 0000-0002-8508-5714

ORCID[3]: 0000-0002-3761-3711

ORCID[4]: 0000-0003-2953-1828

Bu makaleye şu şekilde atıfta bulunabilirsiniz(To cite to this article): Kars Durukan İ., Öztürk M. K. , Özçelik S ve Ozbay E, "Crystal size and stress account in reciprocal space map", ***Politeknik Dergisi***, 22(1): 1-9, (2019).

Erişim linki (To link to this article): http://dergipark.gov.tr/politeknik/archive

DOI: **10.2339/politeknik.417752**

Crystal Size and Stress Account in Reciprocal Space Map

Araştırma Makalesi / Research Article

İlknur KARS DURUKAN[1*], Mustafa Kemal ÖZTÜRK[2,3], Süleyman ÖZÇELİK[2,3], Ekmel ÖZBAY[4]

[1]Department of Physics, Faculty of Sciences, Gazi University, Ankara, Turkey
[2]Photonics Research Center, Gazi University, Ankara, Turkey
[3]Department of Physics, Bilkent University, Bilkent, Ankara

(Geliş/Received : 24.10.2017 ; Kabul/Accepted : 08.02.2018)

ABSTRACT

In this study, five periodic InGaN / GaN LED (light emitting diode) structures grown by the Metal Organic Vapor Deposition (MOCVD) at different active layer growth temperatures were studied. These structures were grown as InGaN / GaN multiple quantum wells (MQW) between c-oriented sapphire substrate and n-GaN and p-AlGaN + GaN contacts. These constructions were characterized by the high-resolution X-ray diffraction (HR-XRD) system. HRXRD patterns obtained by X-ray diffraction and Reciprocal space maps were performed from the same data. One of the most effective ways of studying the crystal lattice is reciprocal space mapping with HR-XRD technique. This technique does not damage the sample. Information can be obtained from the internal system of the sample or from the intermediate layer including substrate. Using the FWHM (β_{hkl}) values and the elastic coefficients of the structures obtained for each of the three samples separately with the inverse mesh technique, D (nm) particle size, σ (GPa) uniform stress, ε strain, u (kJm^{-3}) anisotropic energy density parameters were calculated. These calculations were done in a Scherrer method and Uniform Deformation Model (UDM) which is the Williamson Hall method, modified uniform Williamson stresses model (USDM) and Uniform Deformation Energy Density Model (UDEDM). The results show that the stretching in the crystal size is very little. Line expansion in HR-XRD is due to small crystal size and lattice strain. UDEDM, one of the W-H methods, has emerged as the most suitable model for stretching..

Keywords: : Strain, particle size, Williamson-Hall, reciprocal space mapping.

Ters Örgü Uzayında Kristal Boyutu ve Stres Hesabı

ÖZ

Bu çalışmada, farklı aktif tabaka büyütme sıcaklıklarında MOCVD yöntemi ile büyütülen beş peryotlu InGaN/GaN LED yapıları çalışıldı. Bu yapılar c-yönelimli safir alttaş üzerine n-GaN ve p-AlGaN+GaN kontak arasında olacak şekilde, InGaN/GaN çoklu kuantum kuyu (MQW) olarak büyütüldü. Bu yapılar, HR-XRD sistemi ile karakterize edildi. X-Işını kırınımı ile elde edilen HR-XRD desenleri ve aynı verilerden, Ters Örgü Uzayı Haritalaması yapıldı. Kristal örgüsünün incelenmesinde en etkili yollardan bir tanesi Yüksek çözünürlüklü XRD (HR-XRD) tekniğiyle ters örgü haritalamasıdır. Örneğe zarar vermez. Örneğin iç sistemlerinden veya alttaş dahil arakatman tabakalardan bilgi alınabilir.Ters örgü uzayı tekniği ile her üç numune için ayrı ayrı elde edilen tabakalara ait FWHM (βhkl) değerleri ve yapıların elastik katsayıları kullanılarak; D (nm) parçacık boyutu, σ (GPa) uniform stress, ε strain, u(kJm^{-3}) anisotropic enerji yoğunluğu parametreleri hesaplandı. Bu hesaplamalar; Scherrer yöntemi ve Williamson Hall yöntemi olan Uniform Deformation Model (UDM), modifiye Williamson Hall yöntemleri olan Uniform stress deformation model (USDM) ve Uniform Deformation Energy Density Model (UDEDM) kullanılarak yapıldı. Sonuçlar göstermiştir ki kristal boyutunda gerilme çok az etkilidir. HR-XRD'deki çizgi genişlemesi küçük kristal boyutu ve örgü gerilmesi kaynaklıdır. W-H yöntemlerinden biri olan UDEDM'nin gerilme için en uygun model olduğu ortaya çıkmıştır.

Anahtar kelimeler: Strain, parçacık boyutu, Williamson-Hall, ters örgü uzayı haritası.

1. INTRODUCTION

Nitrogen containing optoelectronic devices, a member of the III-V group of semiconducting compounds, have a profound effect on nanotechnology. The direct band energy ranges of Indium Nitride (InN), gallium nitride (GaN) and Aluminum Nitride (AIN) are 0.7 eV, 3.4 eV and 6.2 eV, respectively. These energy band spacings are very wide ranging from the near infra-red region to the ultraviolet (UV) region of the electromagnetic spectrum [1]. Group III nitrides, especially GaN-based, are important materials in LED structures. Indium gallium nitride (InGaN) LEDs are made resistant to high temperature, pressure and frequency conditions. These materials are traditionally grown on a substrate such as sapphire (Al_2O_3) or silicon (Si). This enlargement results in a high level of non-conformity, which causes the cracks to disintegrate, and the dislocations caused by this discrepancy are in the range of 10^7-10^{11} cm^{-2}[2,3]. The GaN buffer layer is grown between the InGaN / GaN active quantum well layer and the Al_2O_3 substrate to remove the structural defects (one-dimensional and two-dimensional, linear and volumetric defects) common to such structures. This reduces lattice mismatch to be transmitted to the InGaN layer, but cannot completely remove the lattice mismatch. Due to the incompatibility

*Sorumlu Yazar (Corresponding Author)
e-posta : ilknurdurukan@gazi.edu.tr

between the Al_2O_3 and GaN layer, it is inevitable to transmit disturbing dislocations (TD) of $1x10^8$ to $1x10^{12}$ cm^{-2} to the InGaN active layer. Despite all of these drawbacks, it is seen that the performance of optoelectronic devices produced from such nitrile-based semiconductors is better than conventional semiconductors [2-5]. The development of the properties of nitrile-based semiconductors and the work to be done to increase their performance will further improve the performance of these devices and the systems that are integrated with them. The purpose of this study is; In the MOCVD system, the growth characteristics of the $In_xGa_{1-x}N$ /GaN multi-quantum well LED structure are reproduced by increasing the InGaN, GaN and aluminum gallium nitride (AlGaN) the result is to investigate the effect on performance of such devices.

In particular, stress, strain and deformation energy density parameters were calculated semi-experimentally using William-Hall technique.

2. EXPERIMENTAL CONDITIONS

InGaN / GaN LED structure were grown by MOCVD on c-oriented (00.1) Al_2O_3 substrate and given in the Figure 1. The same LED samples were used for stress measurements in our study [7], Here, the growth steps are briefly mentioned. Before the epitaxial growth process was started, the Al_2O_3 substrate was heat treated at 1100 ºC for 10 minutes in a nitrogen atmosphere to remove the oxides from the surface. Following chemical reactions of Trimethylgallium(TmGa), Trimethylaluminum (TmAl), TmIn(Trimethylindium) and NH_3(ammonia) compounds, Ga, Al, In and N sources were obtained, respectively. On Al2O3 substrate under constant pressure at 200 mbar; GaN core layer at 500 ° C, GaN buffer layer at 1020 ° C grown. Subsequently, n-type GaN contact layers; 23 sccm TmGa constant current and at 1030 ºC; the first layer was grown for 35 minutes and the second layer for 20 minutes. Then, at flow rates of 140 sccm TmGa and TmIn; The InGaN active layer of samples A, B, and C was formed as five layers at temperatures of 650 ° C, 667 ° C and 700 ° C for 90 (InGaN layer) and then 390 (GaN layer) seconds, respectively. The GaN cap layer was grown for 390 seconds at 730 ° C in a current of 140 sccm TmGa on active layers. Magnesium (Mg) doped p-contact AlGaN layer using 9 sccm TmGa, 15 sccm TmAl and 90 sccm Cp_2Mg flux ratio; 1085 ºC and 50 mbar pressure for 65 seconds. The growth of the p-GaN layer was performed at a flow rate of 14 sccm TmGa and a flow rate of 100 sccm Cp_2Mg; 1010 ºC and 200 mbar pressure for 720 seconds. NH3 flux ratio; 1300 sccm for the GaN and AlGaN layers, and 5200 sccm for the InGaN / GaN active layer. The grown conditions of the other layers are the same for all samples.

The characterization of the samples were analyzed by the HR-XRD technique using a Bruker D8 system, delivering a $CuK_\alpha 1$

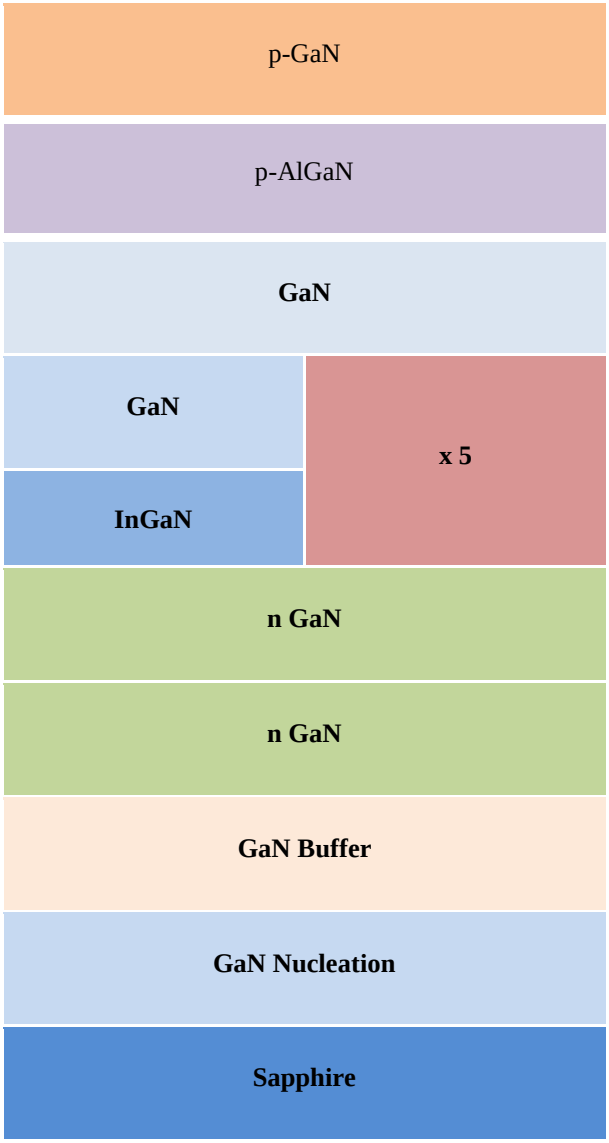

Figure 1. General schematic structure of InGaN / GaN LED structure

3. RESULTS AND DISCUSSION

The Reciprocal space maps obtained by the HR-XRD technique was used to calculate D (nm) particle size, σ (GPa) uniform stress, ε strain, u(kJm^{-3}) anisotropic energy density parameters.

The patterns obtained with the mapping of the reciprocal space provide a more detailed and clearer representation than the classically obtained HR-XRD peaks [6]. The presence of the peaks of the GaN, InGaN and AlGaN layers can be more clearly understood by this mapping. For comparison, the classical HR-XRD pattern for the symmetrical plane of sample B (004) is given in Figure1 in our study [7] and the reciprocal space pattern for the same shot is given in Figure 3-a. In our study, unlike the other study, the stress study was performed with the William Hall method. The our study of the mapping of the reciprocal space of (004) and (106) planes of the samples is given in detail.

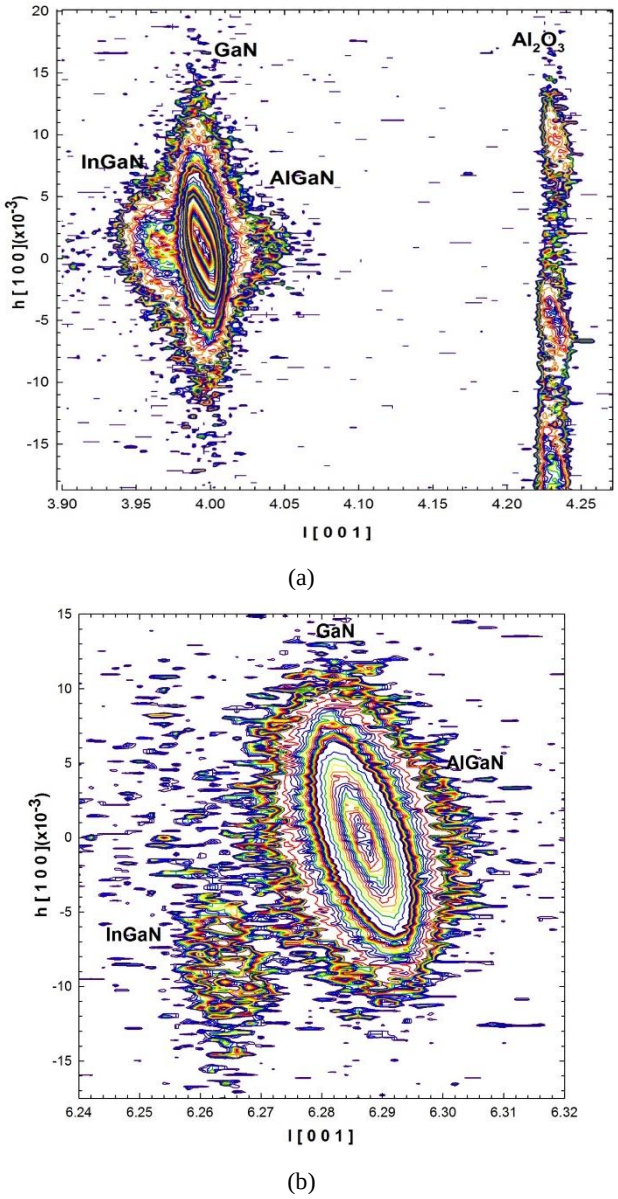

Figure 2. HR-XRD reciproral space mapping of a) (004) and b) (106) miller reflection plane of sample A

When examined in detail in Figure 1[7] in our study, the AlGaN peak, which is not fully separated to the right of the GaN peak, appears to the right of the GaN peak in Figure 3-a. The InGaN peak appears clearly visible and more understandable on the left side of the GaN peak. In addition, SL satellite peaks could be detected quite successfully in the reciprocal space pattern. The HR-XRD reciprocal mesh space pattern of the symmetric miller reflection plane (004) of sample A is given in Figure 2-a. As shown in the figure, it is seen that the Al_2O_3 peak which is used as a substrate on the far right and the peaks of InGaN and AlGaN layers are embedded in the peak of the GaN layer. In Figure 3-b, the reciprocal space mapping pattern of HR-XRD asymmetric plane (106) of sample A is seen. When the pattern is examined, peaks of InGaN partially separated from the GaN peak and peaks of the AlGaN layer not fully decomposed are observed. HR-XRD reciprocal space mapping pattern of the symmetric miller reflection plane (004) of sample B is given in Figure 3-a.

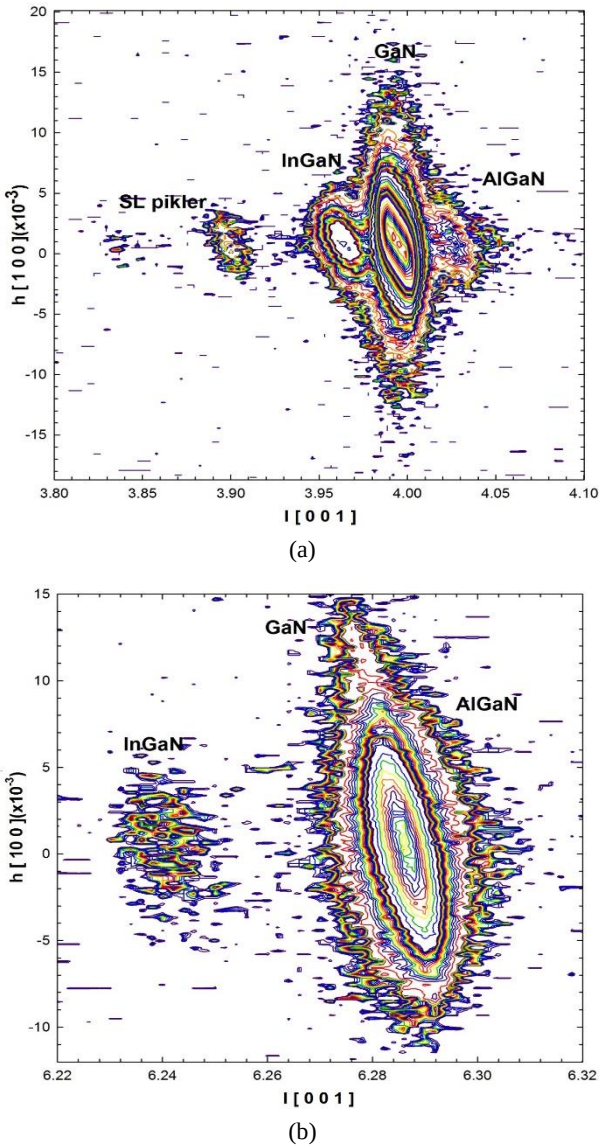

Figure 3. HR-XRD reciprocal space mapping pattern of the symmetric miller reflection plane a)(004) and b)(106) of sample B

SL-2 and SL-1 satellite peaks are seen from the left of the figure. In addition, the InGaN and AlGaN peaks are found somewhat more separated than sample A. Here, symmetric peaks are more intense in the plane of (0004). The initiatives of incoming reflections of the density of GaN and InGaN layers constitute satellite peaks. These satellite peaks are related to crystal quality and surface roughness between layers. Satellite peaks are used to find the thickness of multiple quantum wells. From these satellite peaks, the thickness calculation can be done simply by using the formula [1].

$$T = \lambda / (2 * \Delta\theta * Cos\theta) \quad (1)$$

Here, λ is the wavelength of the X-ray source, Δθ is the satellite peak separation, and θ is the Bragg angle of the plane. A, B and C samples of quantum well thickness are 13.87 nm, 12.58 nm and 10.39 nm, respectively [7]. The quantum well thickness relates to the thickness of GaN and InGaN layers. The two layers have different thicknesses and for this reason X-rays create interference. A quantum well thickness calculation is made from the peak differences of these interference peaks. In other thicknesses, the thicknesses of these layers cannot be determined because density difference and critical thickness are not provided. It was observed that the quantum well thickness decreased with temperature increase. Due to the increased stresses in the structure and the random variation in crystal dimensions, the thickness is affected. The In contents of samples A, B and C with different quantum well thickness are 10.87, 9.01, 7.51, respectively [7]. As the defect density in the structure increases, it decreases the Indium ratio.

The Reciprocal space mapping pattern of the asymmetric reflection planes (106) of sample B, are given in Figure 3-b. it is seen that the AlGaN layer is not fully decomposed while the InGaN layer is distinctly separated from the GaN layer.

Reciprocal space mapping pattern of symmetrical and asymmetric planes of sample C are shown in Fig. 4. When the pattern of symmetric (004) planes is examined, it is seen that the SL-2 and SL-1 peaks are distinctly separated from the left, the InGaN layer has less peaks but the AlGaN layer is more distinct.

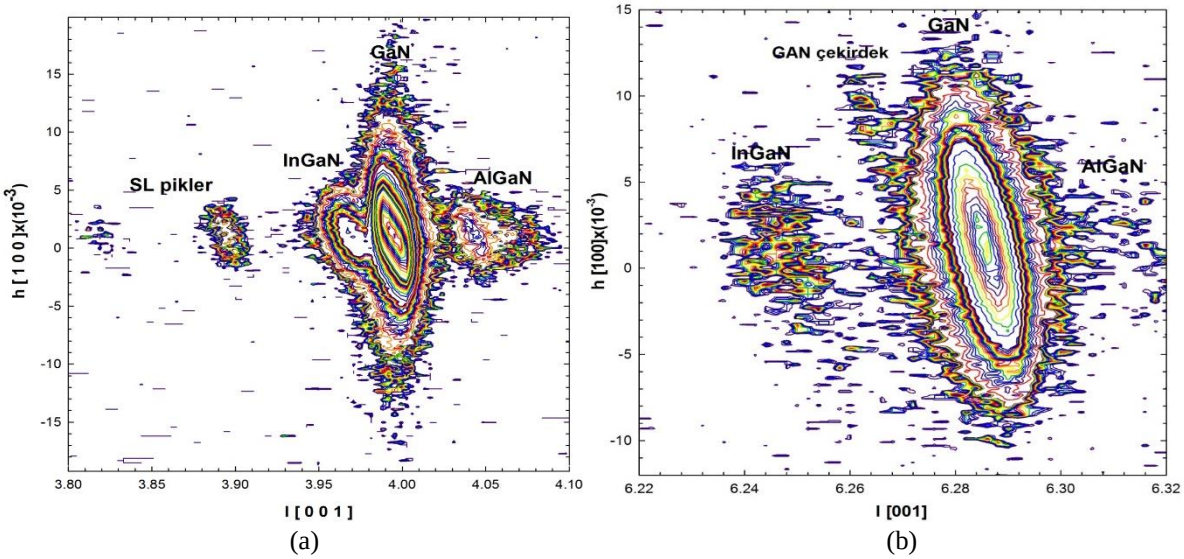

Figure 4. HR-XRD reciprocal space mapping pattern of the symmetric miller reflection plane a)(004) and b)(106) of sample C

When the pattern of symmetrical (004) planes is examined, it is seen that the SL-2 and SL-1 peaks are distinctly separated from the left side, the InGaN layer has less peaks but the AlGaN layer is more distinct. (106) is asymmetric plane pattern is similar to that of the symmetric planes, it is seen that the InGaN layer peaks are distinct but the peaks of the AlGaN layer arenot distinct. Also, It is seen that the peak formations of the GaN core layer are partially formed.

Looking again at Figure 2-a, Figure 3-a and Figure 4-a, The SL peaks are not seen for the A sample, and for the B and C samples, the SL-1 and SL-2 satellite peaks are distinguished from each other and more visible. Because of the increase in roughness between layers, roughness-induced HR-XRD interferences are deteriorating. The absence of the SL-2 satellite peak in sample A shows the roughness between the layers. Therefore, this indicates low crystal quality. The satellite peaks of B and C are more clearly distinguished from each other. The finger peaks between the satellite peaks are weak and it has a less rough layer surface and therefore higher crystal quality than sample A. As a result, the grown temperatures at 667 and 700 ºC have allowed better crystal quality. In addition, in Fig. 2-a for sample A, the peaks of InGaN to the left of the GaN peak and the AlGaN layer to the right are not fully separated. For sample B, the peaks of InGaN to the left of the GaN peak and the AlGaN layer to the right are is more clearly seen in Fig. 3-a. The peak of the InGaN layer on the left side of the GaN peak is partially separated while the peak of the AlGaN layer on the right side is more distinct and separated in sample C. The more pronounced dissociation of the InGaN peak for sample B is due to the increase of the In ratio in the composition, while the more pronounced dissociation of the AlGaN peak in sample C is attributed to the higher Al content in the composition than the sample B [7]. This is related to microstructural imperfections in the complete dissociation of these HR-XRD peaks of the InGaN and AlGaN layers [8-14].

3.1 Crystal Size Account According to Scherrer Method

In order for the Scherrer method to be applied in a healthy way, it is very important to calculate the exact value of

βhkl accurately [15]. Bragg peak patterns obtained by HR-XRD analyzes are dependent on both device and sample effects. The device-corrected enhancement (βhkl) corresponding to each diffraction peak of InGaN is giveby Equation (2) below.

$$\beta_D^2 = \left[(\beta^2)_{numune} - (\beta^2)_{cihaz} \right] \quad (2)$$

The crystal size D, perpendicular to the reflective planes, can be obtained by Equation 3.

$$D = \frac{k\lambda}{\beta_{hkl} \cos\theta} \rightarrow \cos\theta = \frac{k\lambda}{D}\left(\frac{1}{\beta_{hkl}}\right) \quad (3)$$

Here, k is a coefficient; λ, X-ray wavelength; θ is the Bragg angle. By fitting the data, the crystal size D is found from the slope of the fit line. Using the FWHM results calculated from the Reciprocal space maps obtained from the HR-XRD patterns, the Scherrer graph expressing Cosθ versus 1 / β_{hkl} is plotted in Figure 5 for the InGaN, AlGaN and GaN layer. The D crystal size (nm) was calculated from the slope of the fit. The crystal sizes of the InGaN, AlGaN and GaN layers were 35.895, 21.773 and 51.326 nm, respectively. The R^2 compliance value of the graphs varies between 0.1-0.7.

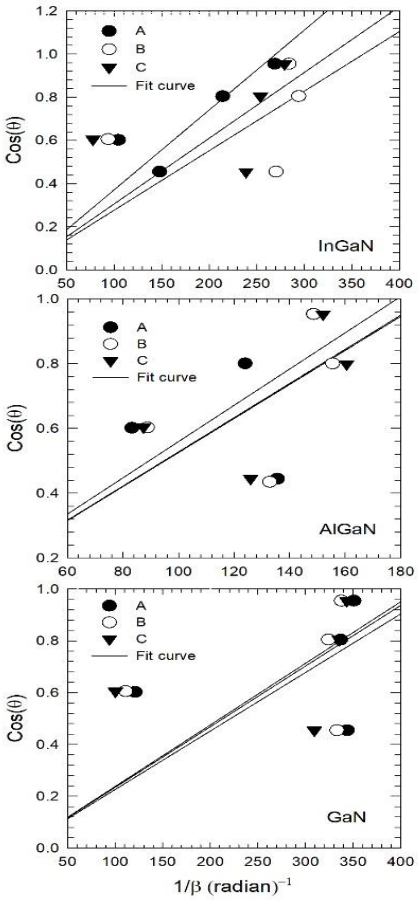

Figure 5. Scherrer chart for InGaN,AlGaN and GaN layer

The Scherrer method is widely used in dust samples. Dust samples are made up of small particles. The peaks must be sufficiently intense to be able to perform the Scherrer analysis. For amorphous materials, there is a limit in the Scherrer equation. We find the planes of semiconductors, and in the case of dust we see the corresponding planes at a certain rate. The W-H equation is a combination of the Scherrer equation and the strain equation. It is widely used in semiconductors. Because of the high level of dislocations in the crystallized layer, mosaic blocks similar to the shape of large radius grains. In this case the parameters(strain, young module, elastic constants) are more stable, it is more accurate to get clear results. Due to the GaN point defects, the FWHM values of the pixels are unstable.

3.2 Crystal Size Account According to W-H Method

In reality, not all materials are perfect crystal. There are absolutely deformations. Strain is a defect that occurs as a result of the crystal being not perfect or lattice force and given by ε≈βs/4tanθ. Peak displacement in the diffraction pattern causes the half-width to change. For the strain calculation, tanθ curves are plotted against βhkl as a linear equation as in particle size calculation. The calculated strain value is not a realistic result as it is in the calculation of the particle size. However, the W-H technique is a very useful technique that distinguishes these two effects from each other. Here, we can talk about three models as W-H.

W-H analyzes in our studies; Uniform Deformation Model (UDM), Uniform Stress Deformation Model (USDM) and Uniform Deformation Energy Density Model (UDEDM). The W-H model is not dependent on 1 / cosθ as in the Scherrer model but varies with tanθ. This main difference distinguishes between the coexistent microstrain and the reflection expansion [16]. Strain occurs without the crystal being perfect and without separation, and can be calculated by Equation 4 [15]. ε is the square root (RMS) value of the square mean of the micro strain.

$$\varepsilon = \frac{\beta_{hkl}}{4\tan\theta} \quad (4)$$

The sum of the strain values of the InGaN and GaN layers is lower than that of the AlGaN layer. This is why the InGaN and GaN layers are better optimized when grown. The AlGaN layer has high dislocation. For this reason, the strain in the AlGaN layer is larger than the quantum well layer.

Figure 6 show tanθ graphs for βhkl of the InGaN, AlGaN and GaN layers, for all three samples. The R^2 compliance value of the graphs varies between 0.1-0.45. The values appearing in this range are consistent with the article results. If $R^2 = 1$, the fit value is perfect compliance value. The values appearing in this range are consistent with the article results. Systematic faults resulting from the system are few, since the angle is calibrated to 0.0005

precision. Low level, the flaws in the sample are more oppressive because they are purely experimental results.

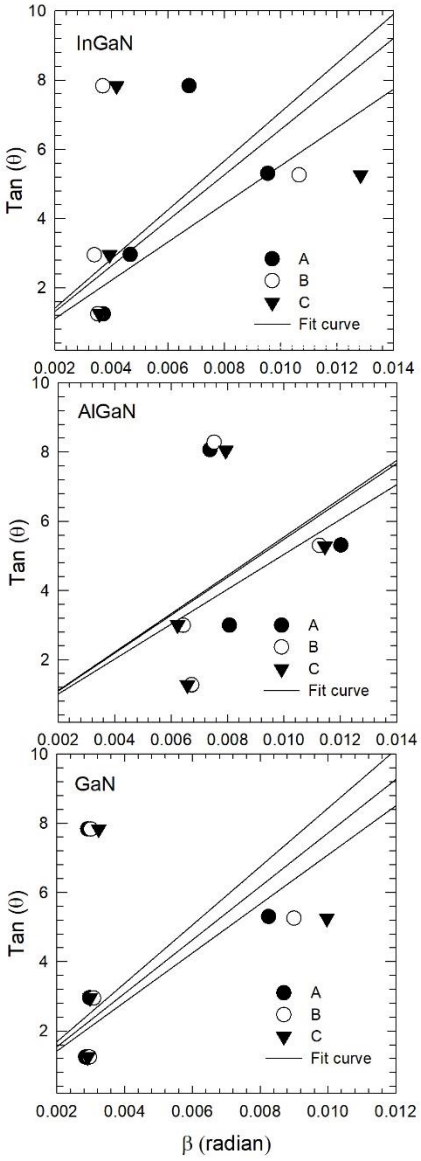

Figure 6. Graphs of Tan(θ) versus βhkl of the InGaN, AlGaN and GaN layer

Strain and particle size are not linearly independent of one another. Thus the peak width of the Bragg reflections is given by the equations below as the sum of the two influencing peak widths.

$$\beta_{hkl} = \beta_1 + \beta_\varepsilon = \left[K\lambda / t\cos\theta_{hkl}\right] + \left[4\varepsilon\tan\theta_{hkl}\right] \quad (5)$$

$$\beta_{hkl}\cos\theta_{hkl} = \beta_1 + \beta_\varepsilon = \left[K\lambda / t\right] + \left[4\varepsilon Sin\theta_{hkl}\right] \quad (6)$$

This equation is known as the classical W-H equation or the uniform deformation model (UDM). In this equation, the crystal strain is crystallographically the same in all directions. Therefore, the crystal is considered as isotropic. When the graph is plotted against $4\sin\theta_{hkl}$ versus βhkl cosθhkl using the planes with the permissible crystal planes, the microstrain is calculated from the slope [15]. Graphs for all three samples were given in Figures 7. The R^2 compliance value of the graphs varies between 0.1-0.23. The values appearing in this range are consistent with the article results. Similar results were obtained for the R^2 values in a study conducted with the W- H technique [17].

The crystal size is also calculated from the y-axis cutting point. Calculated values are given in Tables 3.

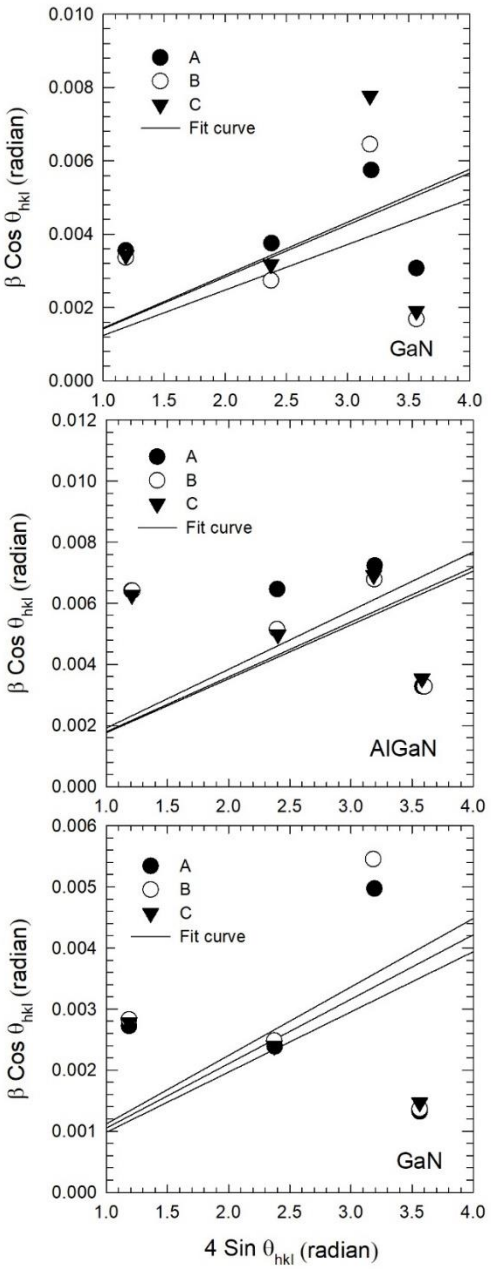

Figure 7. Graph of InGaN, AlGaN and GaN layer according to the UDM model

Due to the high pressure produced in this direction, the diffraction line widens considerably and shifts to a higher d range. This shows the pressure on the lattice of InGaN. The positive value obtained from the graph supports the presence of pressure. In many cases the acceptance of homogeneity and isotrobic. Thus, the USDM and UDEDM methods are more realistic as they account for

the anisotropic structure of the Young modules of crystals [18].

According to USDM method, the cause of anisotropic micro tension (εhkl) is (σ) smooth deformation pressure. Hooke's law expresses the correct proportion (σ=εE$_{hk}$l) between pressure and strain and adding this approach to the account, the W-H equation can be written as Equation 7 [15].

$$\beta_{hkl} = \left(\frac{k\lambda}{D}\right) + \left(\frac{4\sigma \sin\theta}{E_{hkl}}\right) \quad (7)$$

Ehkl shows the Young's modulus perpendicular to the hkl planes, and if the stress is known from the slope of the graph of the 4sinθ / E$_{hkl}$ versus β$_{hkl}$cosθ and the Ehkl is known, the crystal size; can be found from the cut point of the fit line [15].

Universal elastic parameters of InGaN, InN and GaN are given in Table 1

Elastic constants of InGaN are 0.109; 0.090 and 0.080 as calculated by the law of Vegard for sample A, B and C, respectively [6,11].

$$c_0(InGaN) = x\,c_0(InN) + (1-x)\,c_0(GaN) \quad (8)$$

Table 1. Universal elastic constants of InN and GaN, InGaN

	InN	GaN	InGaN		
			A	B	C
C_{11}	190	390	368.26	371.98	374.98
C_{12}	104	145	140.54	141.31	141.92
C_{13}	121	106	107.63	107.35	107.13
C_{33}	182	398	374.52	378.54	381.78
C_{44}	10	105	94.67	96.44	97.87

For a sample in the hexagonal crystal phase, the Young's modulus is given by Equation 9 [19-21].

$$E_{hkl} = \left(h^2 + \frac{(h+2k)^2}{3} + \left(\frac{al}{c}\right)^2\right)^2 X\left[S_{11}\left(h^2 + \frac{(h+2k)^2}{3}\right) + S_{33}\left(\frac{al}{c}\right)^4 + (2S_{13}+S_{44})\left(\left(h^2 + \frac{(h+2k)^2}{3}\right)\left(\frac{al}{c}\right)^2\right)\right]^{-1} \quad (9)$$

s$_{11}$, s$_{12}$, s$_{13}$, s$_{33}$, s$_{44}$ are the elasticity coefficients of InGaN and AlGaN and these calculated values are given in Table 2.

Table 2. Calculated elasticity coefficients for the InGaN and AlGaN layers for all three samples

(GPa^{-1})	A		B		C	
	InGaN	AlGaN	InGaN	AlGaN	InGaN	AlGaN
S_{11}	0.0033	0.0030	0.0033	0.0030	0.0032	0.0030
S_{12}	0.0011	0.0010	0.0011	0.0010	0.0011	0.0010
S_{13}	0.0006	0.0005	0.0006	0.0005	0.0006	0.0005
S_{33}	0.0030	0.0028	0.0030	0.0028	0.0030	0.0028
S_{44}	0.0106	0.0086	0.0104	0.0087	0.0102	0.0086

Figure 8; The W-H method shows a graph of InGaN, AlGaN and GaN layers for all three samples according to the USDM model. The R^2 compliance value of the graphs varies between 0.1-0.3. The values appearing in this range are consistent with the article results.

If values are to be fitted in these graphs, the anisotropic energy density (u) is found from the slope of the fit lines. The crystal size (D) is also found at the y-axis cutting point. Deformation stress and deformation energy density obtained from USDM and UDEDM models can be related to u=σ2/2E$_{hkl}$ expression [15]. Both Equation 8 and Equation 9 are different because they assume that the elasticity constant is anisotropic.

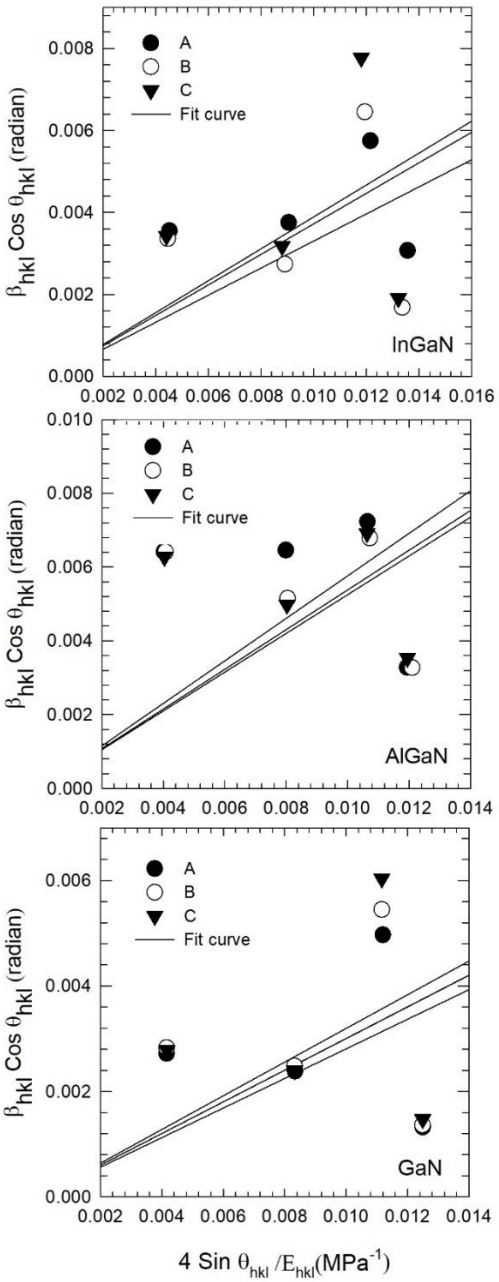

Figure 8. Graph of InGaN, AlGaN and GaN layer according to the USDM model

Because in Equation 8, deformation stress has the same value in all directions and this makes u anisotropic. In Equation 9, deformation energy is assumed to be uniform in all directions. Here, deformation stress σ is anisotropic.

Figure 9; The W-H method shows a graph of of InGaN, AlGaN and GaN layers for all three samples according to the UDEDM model. The R^2 compliance value of the graphs varies between 0.1-0.23. The values appearing in this range are consistent with the article results.

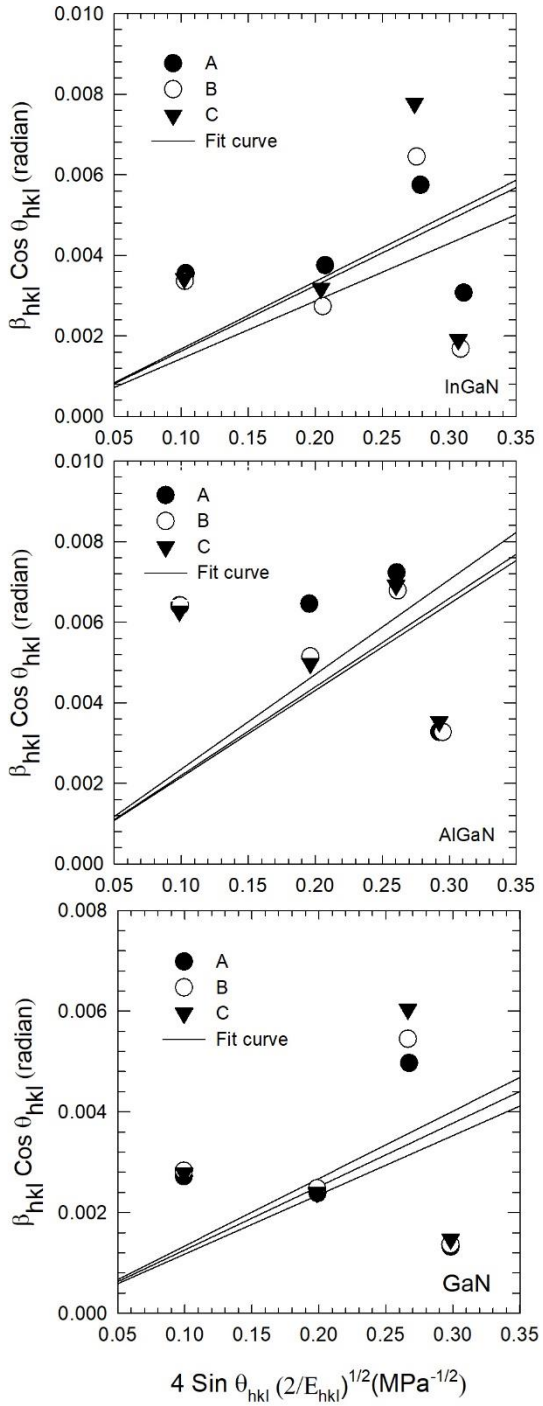

Figure 9. Graph of InGaN, AlGaN and GaN layer according to the UDEDM model

All samples; The results obtained from the Scherrer, UDM, USDM and UDEDM methods are given in Tables 3 for InGaN, AlGaN and GaN layers.

Table 3. Physical parameters calculated for USD, USDM and UDEDM models for all three layers of sample A, B and C

			Sample A			Sample B			Sample C		
			InGaN	AlGaN	GaN	InGaN	AlGaN	GaN	InGaN	AlGaN	GaN
SCHERRER		D(nm) cos θ	36.087	7.366	61.232	48.362	6.319	58.651	43.723	5.468	55.718
		D(nm) sin θ	35.895	21.773	51.326	41.134	21.780	49.270	38.965	21.899	48.625
WH	UDM	D(nm)	47.542	14.031	57.597	48.947	15.019	56.266	51.325	15.414	62.418
		ε x10^{-3}	0.250	2.997	0.021	0.104	2.815	0.066	0.361	2.723	0.230
	USDM	D(nm)	47.542	14.031	57.597	48.947	15.019	56.266	51.325	15.414	62.418
		σ (GPa)	0.066	0.900	0.006	0.028	0.838	0.019	0.097	0.816	0.066
		ε x10^{-3}	0.250	2.997	0.021	0.104	2.815	0.066	0.361	2.723	0.230
	UDEDM	D(nm)	47.542	14.031	57.597	48.947	15.019	56.266	51.325	15.414	62.418
		u(kJm^{-3}) x10^3	0.008	1.348	0.000	0.001	1.180	0.001	0.018	1.112	0.008
		σ (GPa)	0.066	0.900	0.006	0.028	0.838	0.019	0.097	0.816	0.066
		ε x10^{-3}	0.250	2.997	0.021	0.104	2.815	0.066	0.361	2.723	0.230

The results show that the strain is very little effect on the crystal size. The crystal sizes obtained from W-H and Scherer can be compared. In addition, the W-H methods UDM, UDEDM and USDM gave very consistent and similar results. The enlargement of the pikes increases the strain at the large angles and the crystal size decreases accordingly. This is caused by an increase in the reflection angles.

4. CONCLUSION (SONUÇ)

In this study, three five-period InGaN / GaN LED structures were grown by MOCVD at 650, 667 and 700 oC active layer growth temperatures. These structures were characterized by the HR-XRD system. Unlike classical HR-XRD analysis methods, reciprocal space mapping was performed. It can be seen that more detailed and clear results can be obtained with the reciprocal space mapping. Two different methods were used in mosaic structure calculations. William Hall method is common technique for semiconductors and σ (GPa) uniform stress, ε strain, u (kJm^{-3}) anisotropic energy density parameters are calculated. It is important to use XRD by semi-experimental methods instead of expensive and difficult methods such as TEM to analyze defects properties.

Uniform stress (σ) is; with the stain parameter, exhibited exactly the same behavior for all three layers. The anisotropic energy density (u) follows the same regime as the other parameters, exhibiting a decrease and increase then with increasing temperature for the InGaN layer and a continuously decreasing for the AlGaN layer, as opposed to the AlGaN layer, which exhibited increased behavior.

In addition, according to the Scherrer method, for the InGaN layer of sample A, the particle size in the calculations made according to sinθ is 0.5% less than cos

θ, while 15% in case B and 11% in case C are calculated. Similar behavior to the InGaN layer was observed in the GaN layer, which was up to three to four times larger for the AlGaN layer, and this increase was directly proportional to the growth temperature. The line expansion in the HR-XRD was attributed to the small crystal size and lattice strain.

The results showed that; the results obtained with the calculations made are quite consistent with the literature. Both the Scherrer and W-H methods are close to each other, and the W-H methods UDM, USDM and UDEDM are very consistent with each other. Among these methods, the UDEDM method is a suitable metric for the calculation of strain and other parameters..

REFERENCES

[1]. Morkoç, H., "***Hand book of Nitride Semiconductors and Devices***", Wiley-VCH, 16. Berlin, (2008).

[2]. Kapolnek, D., Wu, X. H., Heying,B., Keller, S., Keller, B. P., Mishra, U. K., Den Baars, S. P. and Speck, J. S. "Structural evolution in epitaxial metalorganic chemical vapor deposition grown GaN films on sapphire", ***Applied Physics Letters***, 67(11): 1541-1543, (1995).

[3]. Ponce, F. A., Krusor, B. S., Jr, J. S. M., Plano, W. E. and Welch, J. "Microstructure of GaN epitaxy on SiC using AlN buffer layers", ***Applied Physics Letters***, 67(3): 410-412, (1995).

[4]. Chichibu, S., Azuhata, T., Sota, T., Nakamura, S. "Spontaneous emission of localized excitons in InGaN single and multiquantum well structures", ***Applied Physics Letters***, 69(27): 4188-4190, (1996).

[5]. Lester, S. D., Ponce, F. A., Crawford, M. G., Steigerwald, D. A. "High Dislocation Densities in High-Efficiency Gan-Based Light-Emitting-Diodes", ***Applied Physics Letters***, 66(10): 1249-1251, (1995).

[6]. Baş, Y. "InxGa1-xN (x= 0,075; 0,090; 0,100) "Mavi LED'lerin Mikroyapısal Kusurlarının Ters Örgü Uzay Haritası İle İncelenmesi", Doktora Tezi, Gazi Üniversitesi Fen Bilimleri Enstitüsü, Ankara, (2015).

[7]. Baş, Y., Demirel, P., Akın, N., Başköse, C., Özen, Y., Kınacı B., Öztürk, M.K., Özçelik, S., Özbay, E. "Microstructural defect properties of InGaN/GaN blue light emitting diode structures", ***Journal of Materials Science: Materials in Electronics***, 25(9): 3924-393, (2014).

[8]. Moram, M. A.,Vickers, M. E. "X-ray diffraction of III-nitrides", ***Reports on Progress in Physics***, 72(3): 036502-036541, (2009).

[9]. Öztürk, M. K., Yu, H., Sarıkavak, B., Korçak, S., Özçelik, S., Özbay, E. "Structural analysis of an InGaN/GaN based light emitting diode by X-ray diffraction", ***Journal of Materials Science: Materials in Electronic***, 21(2): 185-191, (2010).

[10]. Öztürk, M. K., Altuntaş, H., Çörekçi, S., Hongbo, Y., Özçelik, S. and Özbay E. "Strain-Stress analysis of AlGaN/GaN heterostructures with and without an AlN suffer and Interlayer", ***Strain***, 47(2): 19-27, (2011).

[11]. Kisielowski, C. "Strain in GaN thin films and heterostructures", ***Semiconductors and Semimetals***, 57(GaN II): 275-317, (1999).

[12]. Çetin, S. S., Öztürk, M. K., Özçelik, S., Özbay, E. "Strain analysis of InGaN/GaN multi quantum well LED structures", ***Crystal Research and Technology***, 47(8): 824-833, (2012).

[13]. Yıldız, A., Öztürk, M. K., Bosi, M., Özçelik, S., Kasap, M. "Structural, electrical and optical characterization of InGaN layers grown by MOVPE", ***Chinese Physics B***, 18(9): 4007-4012, (2009).

[14] Öztürk, M. K., Çörekçi, S., Tamer, M., Çetin, S. Ş., Özçelik, S., Özbay E. "Microstructural properties of InGaN/GaN light-emitting diode structures with different In content grown by MOCVD", ***Applied Physics A-Materials Science&Processing***, 114(4): 1215-1221, (2014).

[15]. Singla, G., Singh, K., Pandey, O. P. "Williamson–Hall study on synthesized nanocrystalline tungsten carbide (WC)", ***Applied Physics A***, 113(1): 237–242, (2013).

[16]. Khorsand Zak, A., Majid, W.H.A., Abrishami, M.E., Yousefi, R. "X-ray analysis of ZnO nanoparticles by Williamson-Hall and size-strain plot methods", ***Solid State Sci.***, 13: 251, (2011).

[17]. Prabhu, Y. T., Rao, K. V., Kumar, V. S. S., Bandla Siva Kumari, "X-Ray Analysis by Williamson-Hall and Size-Strain Plot Methods of ZnO Nanoparticles with Fuel Variation",***World Journal of Nano Science and Engineering***, 4: 21-28, (2014).

[18]. Rosenberg, Y., Machavariant, V.S., Voronel, A., Garber, S., Rubshtein, A., Frenkel, A.I., Stern, E.A. "Strain energy density in the x-ray powder diffraction from mixed crystals and alloys", ***J. Phys. Condens. Matter***, 12: 8081, (2000).

[19]. Warren, B.E., Averbach, B.L." The Effect of Cold-Work Distortion on X-Ray Patterns", ***J. Appl. Phys***., 21: 595, (1950).

[20]. Zang, J., Zhang, Y., Xu, K.W., Ji, V. "General compliance transformation relation and applications for anisotropic hexagonal metals", ***Solid State Commun.***, 139: 87, (2006).

[21]. Balzar, D., Ledbetter, H. J. "Voigt-function modeling in Fourier analysis of size- and strain-broadened X-ray diffraction peaks", ***Appl. Crystallogr.***, 26: 97,(1993).